Icarus 208 (2010) 789–797

Contents lists available at ScienceDirect

Icarus

journal homepage: www.elsevier.com/locate/icarus

A coordinated spectral, mineralogical, and compositional study of ordinary chondrites

Tasha L. Dunn [a,d,*], Timothy J. McCoy [b], J.M. Sunshine [c], Harry Y. McSween Jr. [a]

[a] Department of Earth and Planetary Sciences, Planetary Geosciences Institute, University of Tennessee, Knoxville, TN 37902, USA
[b] Department of Mineral Sciences, National Museum of Natural History, Smithsonian Institution, Washington, DC 20013-7012, USA
[c] Department of Astronomy, University of Maryland, College Park, MD 20742-2421, USA
[d] Department of Geography–Geology, Illinois State University, Normal, IL 61761, USA

ARTICLE INFO

Article history:
Received 12 November 2009
Revised 23 February 2010
Accepted 23 February 2010
Available online 12 March 2010

Keywords:
Asteroids
Spectroscopy
Meteorites

ABSTRACT

Mineral compositions and abundances derived from visible/near-infrared (VIS/NIR or VNIR) spectra are used to classify asteroids, identify meteorite parent bodies, and understand the structure of the asteroid belt. Using a suite of 48 equilibrated (types 4–6) ordinary (H, L, and LL) chondrites containing orthopyroxene, clinopyroxene, and olivine, new relationships between spectra and mineralogy have been established. Contrary to previous suggestions, no meaningful correlation is observed between band parameters and cpx/(opx + cpx) ratios. We derive new calibrations for determining mineral abundances (ol/(ol + px)) and mafic silicate compositions (Fa in olivine, Fs in pyroxene) from VIS/NIR spectra. These calibrations confirm that band area ratio (BAR) is controlled by mineral abundances, while Band I center is controlled by mafic silicate compositions. Spectrally-derived mineralogical parameters correctly classify H, L and LL chondrites in ~80% of cases, suggesting that these are robust relationships that can be applied to S(IV) asteroids with ordinary chondrites mineralogies. Comparison of asteroids and meteorites using these new mineralogical parameters has the advantage that H, L and LL chemical groups were originally defined on the basis of mafic silicate compositions.

1. Introduction

Over the past few decades, an ongoing debate has centered on the identities of the ordinary chondrite parent bodies, the most common meteorites seen to fall to Earth. While earlier workers posited that ordinary chondrite-like bodies should be common in the asteroid belt, it is now generally recognized that only three parent bodies are required to account for the chemically-distinct H, L and LL chondrites. Each chondrite group is chemically homogenous (Dodd, 1981), oxygen isotopes cluster within a narrow range (Clayton et al., 1991), and radiometric ages indicate that many H and L chondrites were ejected from the same parent body (Keil et al., 1994). Visible/near-infrared spectra have been the most widely-applied tool used in the search for these parent asteroids, due to the strong 1 μm and/or 2 μm absorption bands present in the dominant chondritic minerals olivine and pyroxene (Adams, 1974, 1975; Burns et al., 1972; Cloutis, 1985; Cloutis and Gaffey, 1991). This approach requires a direct comparison of spectral band parameters (e.g., Band I and II centers, band area ratios) between meteorite and asteroids. However, if robust relationships between these spectral parameters and mineralogical parameters (abundances and compositions) could be established, these comparisons could be made using the same criteria that are used in meteoritics. Such a comparison has the advantage that the H, L and LL chemical groups were originally defined on the basis of bulk chemistry, particularly total iron abundance and mafic silicate compositions, and not on spectral parameters. The H, L and LL chondrite groups exhibit distinct compositional hiatuses, particularly with respect to mafic silicate compositions, although some authors have questioned whether L and LL chondrites are transitional (Rubin, 1990).

In this paper, we revisit spectral calibrations for asteroids using a data set of 48 measured ordinary chondrite modal abundances and corresponding silicate mineral analyses, which represent the complete petrologic range of the equilibrated ordinary chondrites (types 4–6) (Van Schmus and Wood, 1967). This is the first study in which spectral calibrations have been derived using actual measured ordinary chondrite modal abundances. Prior to this study, spectral calibrations were based on simple mixtures of mafic silicates (Cloutis et al., 1986) or normative abundances of ordinary chondrites (Burbine et al., 2003), due to the difficulty associated with quantifying modal abundances of fine-grained samples. Normative mineralogies are calculated from bulk chemistry using a standard CIPW (Cross, Iddings, Pirsson, and Washington) algorithm (Cross et al., 1902), and are used most often to determine abundances of fine

* Corresponding author at: Department of Geography–Geology, Illinois State University, Normal, IL 61761, USA.
E-mail address: tldunn@ilstu.edu (T.L. Dunn).

0019-1035/$ - see front matter © 2010 Elsevier Inc. All rights reserved.
doi:10.1016/j.icarus.2010.02.016

grained terrestrial samples, such as volcanic rocks. Our new calibrations based on measured abundances should yield more accurate mineralogical interpretations of asteroid spectra.

2. Background

The primary diagnostic feature in olivine is a composite absorption feature at ~1 μm, which consists of three distinct absorption bands. The composite 1 μm band, which is attributed to electronic transitions of Fe^{2+} occupying both the M1 and M2 crystallographic sites (Burns, 1970), moves to longer wavelengths as FeO content increases (King and Ridle, 1987; Sunshine and Pieters, 1998). Pyroxenes have two absorption bands at ~1 μm and ~2 μm that are associated with crystal field transitions in Fe^{2+}, which preferentially occupy the M2 site (Clark, 1957; Burns, 1970). Low-calcium pyroxenes, which are conventionally defined as having less than 11 mol% $CaSiO_3$ (wollastonite or Wo) (Adams, 1974), show a well-defined relationship between absorption band positions and composition, as both Band I and Band II positions increase with increasing ferrous iron content (Adams, 1974; Burns et al., 1972; Cloutis, 1985). There is also a correlation between composition and band positions in high-calcium pyroxene, although the relationship is complicated by the presence of calcium in addition to iron.

In spectra containing both olivine and pyroxene absorptions, the combined absorption features near 1 μm (Band I) and near 2 μm (Band II) are also sensitive to the relative proportions of olivine and pyroxene. The ratio of the areas of these two bands (Band II/Band I) is commonly used to estimate olivine and pyroxene abundances in meteorites and asteroids (Cloutis et al., 1986). The linear relationship between this band area ratio (BAR) and the ratio of pyroxene to olivine + pyroxene (px/(ol + px)) was first recognized Cloutis et al. (1986), who expressed this relationship as

$$\mathrm{BAR} = 0.024 \times (\mathrm{px}/(\mathrm{ol} + \mathrm{px})) - 1.25. \quad (1)$$

While Cloutis et al. (1986) utilized this equation to derive BARs from mixtures of known mineral proportions, Gastineau-Lyons et al. (2002) used this relationship to derive mineral abundances from BARs of asteroid spectra, recasting the Cloutis et al. (1986) calibration as

$$\mathrm{px}/(\mathrm{ol} + \mathrm{px}) = 0.417 \times \mathrm{BAR} + 0.052. \quad (2)$$

However, because the Cloutis et al. (1986) regression was based on simple mixtures of olivine and orthopyroxene, the presence of more than one pyroxene (or other additional phases) would complicate spectral interpretations of asteroids made using this calibration (Gaffey et al., 1993; Sunshine et al., 2004).

In an attempt to determine the mineralogy of the S-type asteroids, Burbine et al. (2003) used normative abundances of the ordinary chondrites, which contain olivine, orthopyroxene and clinopyroxene, to derive a relationship between BAR and ol/(ol + px). Burbine et al. (2003) expressed their equation as

$$\mathrm{ol}/(\mathrm{ol} + \mathrm{px}) = -0.228 \times \mathrm{BAR} + 0.768. \quad (3)$$

The Burbine et al. (2003) calibration yields ordinary chondrite ol/(ol + px) ratios that fall within the same general range of ol/(ol + px) ratios measured from normative mineral abundances of ordinary chondrites (McSween et al., 1991). However, there are systematic differences between the two data sets.

3. Analytical methods

A total of 48 ordinary chondrite samples representing each of the ordinary chondrites groups (H, L, and LL) and petrologic categories 4–6 (Van Schmus and Wood, 1967) were selected for analysis. To ensure that samples represented a single petrographic type, visibly polymict samples were excluded from the study, and only unbrecciated falls with minimal terrestrial weathering were selected for analysis. Reflectance spectra of ordinary chondrites were acquired using a bidirectional spectrometer at Brown University's Keck/NASA Reflectance Experiment Laboratory (RELAB) (Pieters and Hirio, 2004). Spectra of 37 chondrite falls in this study (samples with RELAB IDs TB-TJM-XXX; Table 1) were collected by Burbine et al. (2003) from powders originally prepared for bulk chemical analysis by Jarosewich as part of the Smithsonian Institution's Analyzed Meteorite Powder Collection. Small chips of the remaining 11 chondrites (samples TH-HYM-XXX; Table 1) were acquired from the Natural History Museum in London and from the Smithsonian Institution. Consistent with sample preparation described in Burbine et al. (2003), samples were ground with mortar and pestle into a fine powder (<~150 μm), and the metal fraction of the samples was then magnetically removed from the powder in preparation for spectral analysis. Only the silicate portion of each sample was analyzed. Although removing metal from the sample may alter the slope of the spectrum, it should not affect silicate spectral features (i.e. BAR, Band I or Band II center) or spectrally-derived silicate mineral abundances.

For the 11 chondrites obtained for this study (TH-HYM-XXX; Table 1), availability of material was limited, and the mass of material used to prepare these samples was significantly smaller than the multi-gram masses used by Jarosewich (1990, 2006). It is possible that these powders may not be as representative as those prepared by Jarosewich (1990, 2006), but they were necessary to ensure that the H, L, and LL ordinary chondrite groups were equally represented. Unrepresentative sample powders may be expected to yield modal abundances that are higher or lower than actual values, thereby skewing trends based on modal data. For example, measured abundances of low-Ca pyroxene in two L5 chondrites with limited material (Ausson and Blackwell) are 1–2 wt.% higher than abundances in the remaining L5 chondrites. This results in ol/(ol + px) ratios that are lower than those of the remaining L5 chondrites. However, most samples obtained for this study do not appear to show anomalous modal abundances, and it is unlikely that a few potentially unrepresentative samples would alter conclusions based on 48 samples.

Spectra for all 48 samples were collected over a range of 0.32–2.55 μm at a sampling interval of 0.01 μm. An incident angle of 30° and an emission angle of 0° were used for spectral measurements. Band area ratios and band centers were determined by first dividing out a straight-line continuum using points on either side of Band I and Band II (with 2.5 μm as the furthest data point). The area of each band was measured as the area between the absorption band and a tangent line drawn between two peaks on either side of the absorption, and the band area ratio (BAR) was calculated by dividing the area of Band II by the area of Band I. The average error associated with BAR is 0.01 μm. Band center was determined by fitting a second order polynomial to the bottom of the continuum removed feature, and the minimum point of the polynomial was used as the band center. The uncertainty of band centers is typically between 0.01 and 0.03 μm, with an average error of 0.02 μm. Classifications, grain sizes, and spectral parameters (BCI, BCII, and BAR) are listed in Table 1.

XRD data were collected using an INEL curved position-sensitive detector (PSD) at the Natural History Museum in London, England. Mineral abundances were determined using a whole-pattern XRD fitting procedure, first introduced by Cressey and Schofield (1996) and further developed by Batchelder and Cressey (1998). Experimental configurations and a detailed description of the XRD fitting procedure are reported in Dunn et al. (2010a). Olivine and low-Ca pyroxene compositions in 38 of the ordinary chondrites in this study were determined using a Cameca SX-50 electron microprobe

Table 1
Meteorites measured in this study and their spectral parameters.

Meteorite	Type	RELAB ID[a]	Grain size	Band I (μm)	Band II (μm)	BAR
Bernares (a)	LL4	MT-HYM-083	<150 μm	1.008	1.984	0.522
Greenwell Springs	LL4	TB-TJM-075	<150 μm	0.991	1.959	0.512
Hamlet	LL4	MT-HYM-075	<150 μm	0.980	1.974	0.561
Witsand Farm	LL4	MT-HYM-076	<150 μm	1.004	2.001	0.457
Aldsworth	LL5	MT-HYM-077	<150 μm	0.977	1.960	0.561
Alta'ameem	LL5	MT-HYM-078	<150 μm	0.986	1.952	0.435
Olivenza	LL5	MT-HYM-085	<150 μm	1.012	1.969	0.387
Paragould	LL5	MT-HYM-079	<150 μm	0.985	1.968	0.409
Tuxtuac	LL5	MT-HYM-080	<150 μm	1.035	1.950	0.310
Bandong	LL6	TB-TJM-067	<150 μm	1.001	1.987	0.274
Cherokee Springs	LL6	TB-TJM-075	<150 μm	0.989	1.940	0.406
Karatu	LL6	TB-TJM-077	<75 μm	1.006	1.992	0.311
Saint-Séverin	LL6	TB-TJM-145	<150 μm	1.003	1.881	0.269
Attarra	L4	TB-TJM-065	<150 μm	0.957	1.927	0.726
Bald Mountain	L4	TB-TJM-102	<150 μm	0.929	2.001	0.960
Rio Negro	L4	TB-TJM-081	<150 μm	0.953	1.932	0.813
Rupota	L4	TB-TJM-121	<150 μm	0.955	1.951	0.582
Ausson	L5	MT-HYM-084	<150 μm	0.930	1.918	1.031
Blackwell	L5	MT-HYM-081	<150 μm	0.955	1.953	0.526
Cilimus	L5	MT-HYM-082	<150 μm	0.950	1.925	0.515
Guibga	L5	TB-TJM-134	<150 μm	0.962	1.943	0.633
Mabwe-Khoywa	L5	TB-TJM-107	<150 μm	0.954	1.944	0.744
Malakal	L5	TB-TJM-109	<150 μm	0.954	1.977	0.709
Messina	L5	TB-TJM-099	<150 μm	0.959	1.960	0.595
Apt	L6	TB-TJM-064	<150 μm	0.963	1.940	0.511
Aumale	L6	TB-TJM-101	<150 μm	0.960	1.946	0.614
Karkh	L6	TB-TJM-137	<150 μm	0.964	1.930	0.371
Kunashak	L6	TB-TJM-139	<150 μm	0.972	1.942	0.518
Kyushu	L6	TB-TJM-140	<150 μm	0.970	1.933	0.544
New Concord	L6	TB-TJM-130	<150 μm	0.960	1.928	0.606
Farmville	H4	TB-TJM-128	<150 μm	0.939	1.928	0.789
Forest Vale	H4	TB-TJM-093	<75 μm	0.937	1.934	0.800
Kabo	H4	TB-TJM-136	<150 μm	0.939	1.934	0.915
Marilia	H4	TB-TJM-078	<150 μm	0.934	1.945	0.851
São Jose do Rio Preto	H4	TB-TJM-082	<150 μm	0.942	1.901	0.992
Allegan	H5	TB-TJM-104	nm	0.930	1.897	1.068
Ehole	H5	TB-TJM-074	<150 μm	0.940	1.945	0.999
Itapicuru-Mirim	H5	TB-TJM-097	<150 μm	0.944	1.922	0.878
Lost City	H5	TB-TJM-129	<150 μm	0.940	1.936	0.857
Primbram	H5	TB-TJM-143	<150 μm	0.940	1.906	0.857
Schenectady	H5	TB-TJM-083	<150 μm	0.937	1.913	0.786
Uberaba	H5	TB-TJM-085	<150 μm	0.945	1.943	0.881
Andura	H6	TB-TJM-088	<75 μm	0.927	1.929	0.889
Bustura	H6	TB-TJM-069	<150 μm	0.936	1.918	0.795
Canon City	H6	TB-TJM-131	<150 μm	0.953	1.932	0.752
Chiang Khan	H6	TB-TJM-132	<150 μm	0.946	1.920	0.846
Guarena	H6	TB-TJM-094	<150 μm	0.938	1.916	0.748
Ipiranga	H6	TB-TJM-135	<150 μm	0.939	1.921	0.835

[a] Spectra are available on the RELAB database at http://www.planetary.brown.edu/relabdata/.

at the University of Tennessee. Silicate mineral analyses and a detailed discussion of experimental configurations are provided in Dunn et al. (2010b).

4. Results

4.1. Olivine and pyroxene abundances

XRD-measured abundances of olivine, orthopyroxene, clinopyroxene, and pigeonite (reported as ol/(ol + px)) are presented in Table 2, along with ol/(ol + px) ratios calculated from CIPW norms (McSween et al., 1991) using the bulk chemical analyses of Jarosewich (1990, 2006). The average error associated with XRD-measured ol/(ol + px) ratios is 0.03, which is based on the uncertainty in determination of olivine and pyroxene abundances (±2 wt.%) (Dunn et al., 2010a). The average uncertainty for normative ratios is cited as 0.01 by Burbine et al. (2003). XRD-measured weight ratios of ol/(ol + px) differ slightly from those calculated using normative abundances due to systematic differences between normative and XRD-measured abundances, particularly in olivine and high-Ca pyroxene. Normative olivine abundances are higher than XRD-derived abundances of olivine by an average of 3 wt.%, while normative high-Ca pyroxene abundances are lower by an average of 2.7 wt.%.

The disparity between silicate abundances is a result of the way in which CIPW normative phases are calculated. Because normative abundances are calculated as a limited set of ideal minerals, minerals that are present in a sample may be incorrectly calculated during the CIPW norm procedure if that phase is not a possible normative mineral. Ordinary chondrites contain three pyroxenes: enstatite, diopside, and pigeonite (Wo_{5-20}). Enstatite and diopside are normative phases, but pigeonite is not. As a result, the oxides associated with pigeonite (primarily FeO and MgO) are incorrectly allocated in the CIPW norm calculation. A comparison of normative mineralogies (McSween et al., 1991), electron microprobe-measured chondrite abundances (Gastineau-Lyons et al., 2002), and our XRD-measured abundances suggests that these oxides are incorrectly allocated to olivine, resulting in overestimated normative olivine abundances and lower than expected high-Ca pyroxene

Table 2
ol/(ol + px) ratios derived from XRD, normative, and spectral data.

Meteorite	Type	ol/(ol + px) (XRD)	ol/(ol + px) (norm)[a]	ol/ol + px (spectra)[b]
Bernares (a)	LL4	0.58	–	0.60
Greenwell Springs	LL4	0.64	0.66	0.60
Hamlet	LL4	0.62	–	0.59
Witsand Farm	LL4	0.65	–	0.62
Aldsworth	LL5	0.65	–	0.59
Alat'ameen	LL5	0.62	–	0.62
Olivenza	LL5	0.64	0.67	0.63
Paragould	LL5	0.65	–	0.63
Tuxtuac	LL5	0.63	–	0.65
Bandong	LL6	0.66	0.73	0.66
Cherokee Springs	LL6	0.67	0.68	0.63
Karatu	LL6	0.69	0.72	0.65
Saint-Séverin	LL6	0.65	0.70	0.66
Attarra	L4	0.56	0.62	0.55
Bald Mountain	L4	0.55	0.56	0.50
Rio Negro	L4	0.55	0.59	0.53
Rupota	L4	0.57	0.58	0.59
Ausson	L5	0.55	0.64	0.48
Blackwell	L5	0.56	–	0.60
Cilimus	L5	0.58	–	0.60
Guibga	L5	0.58	0.60	0.57
Mabwe-Khoywa	L5	0.58	0.60	0.55
Malakal	L5	0.57	0.60	0.56
Messina	L5	0.57	0.60	0.58
Apt	L6	0.56	0.67	0.60
Aumale	L6	0.59	0.60	0.58
Karkh	L6	0.59	0.65	0.64
Kunashak	L6	0.60	0.63	0.60
Kyushu	L6	0.61	0.61	0.60
New Concord	L6	0.60	0.64	0.58
Farmville	H4	0.46	0.51	0.54
Forest Vale	H4	0.48	0.57	0.53
Kabo	H4	0.46	0.51	0.51
Marilia	H4	0.46	0.49	0.52
São Jose do Rio Preto	H4	0.46	0.54	0.49
Allegan	H5	0.47	0.48	0.47
Ehole	H5	0.51	0.55	0.49
Itapicuru-Mirim	H5	0.53	0.50	0.52
Lost City	H5	0.49	0.54	0.52
Primbram	H5	0.49	0.51	0.52
Schenectady	H4	0.54	0.59	0.54
Uberaba	H5	0.51	0.56	0.51
Andura	H6	0.53	0.60	0.51
Bustura	H6	0.51	0.53	0.54
Canon City	H6	0.54	0.53	0.55
Chiang Khan	H6	0.53	0.53	0.52
Guarena	H6	0.60	0.54	0.55
Ipiranga	H6	0.52	0.53	0.53

[a] From McSween et al. (1991); – indicates that a norm has not been calculated.
[b] Errors are 0.03 for XRD-measured ratios, 0.01 for normative ratios, and 0.03 for spectral ratios.

(Dunn et al., 2010a). Due to the absence of pigeonite from the set of ideal normative minerals, ratios of ol/(ol + px) calculated using normative abundances (Burbine et al., 2003) are not representative of ordinary chondrite mineralogies and do not provide the most accurate calibration for spectral abundances.

Because the CIPW norm is not well-suited for ordinary chondrites, we derived a new equation for determining ol/(ol + px) ratios from spectra using XRD-measured modal abundances. Linear regression of ol/(ol + px) modal ratios as a function of BARs is presented in Fig. 1a. A least-squares fit of the data yields

$$\mathrm{ol}/(\mathrm{ol}+\mathrm{px}) = -0.242 \times \mathrm{BAR} + 0.728, \quad (4)$$

with an R^2 value of 0.73, which is higher than that of Burbine et al. (2003). The authors would like to note that although the published R^2 in Burbine et al. (1993) is 0.93, the correct value is 0.61 (Burbine, personal communication). ol/(ol + px) ratios derived from reflectance spectra using Eq. (4) are presented in Table 2. The root mean square error of the spectrally derived ol/(ol + px) ratios is 0.03. Fig. 1b compares spectrally-derived and XRD-measured ol/(ol + px) ratios.

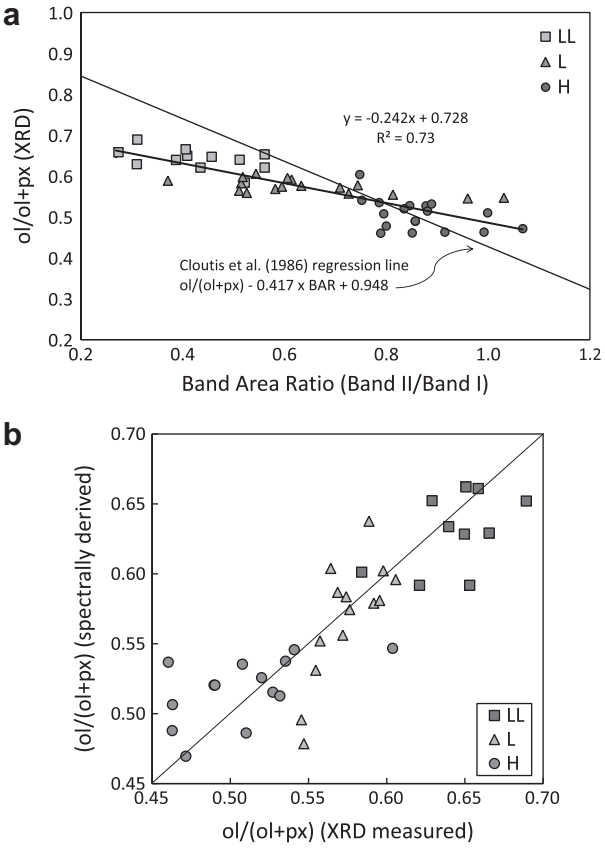

Fig. 1. (a) Linear regression (indicated by bolded black lines) of band area ratios vs. XRD-measured ol/(ol + px) ratios. The solid grey lines are from Cloutis et al. (1986). Error bars are not shown for clarity. (b) XRD-measured ol/(ol + px) ratios vs. spectrally-derived ol/(ol + px) ratios for the ordinary chondrites in this study. The solid diagonal line represents a 1:1 measured to derived ratios. Uncertainties are stated in Table 2.

4.2. Low- and high-Ca pyroxene abundances

Gaffey et al. (2002) suggested that mafic silicate abundances can be constrained even further by considering the effect of high-Ca pyroxene on the Band II position, which they suggested is an almost linear function of the relative abundance of the two pyroxenes. This assertion requires that the cpx/(opx + cpx) ratio is well-correlated with Band II center in the range of values found in ordinary chondrites. Gaffey et al. (2002) derived cpx/(opx + cpx) ratios from spectra, but did not provide a calibration for this calculation. Using XRD-measured pyroxene abundances and Band II centers, we have derived an equation for establishing the ratio of high-Ca pyroxene to total pyroxene. A least-squares fit of the data yields

$$\mathrm{cpx}/(\mathrm{opx}+\mathrm{cpx}) = 0.533 \times \text{Band II center} - 0.795, \quad (5)$$

with a very low R^2 value of 0.15. The remarkably low R^2 value indicates this correlation is poorly constrained. This relationship appears to be even less valid for normative cpx/(cpx + opx) ratios, which yield an R^2 value of only 0.09. XRD-measured cpx/(opx + cpx) ratios, normative ratios, and ratios derived from reflectance spectra are presented in Table 3. These results indicate that there is no significant correlation between Band II position and relative pyroxene abundance. We conclude that Band II should not used to derive

Table 3
XRD-measured, normative, and spectral cpx/(opx + cpx) ratios.

Meteorite	Type	cpx/(opx + cpx) XRD	cpx/(opx + cpx) norm[a]	cpx/(opx + cpx) spectra
Bernares (a)	LL4	0.29	–	0.26
Greenwell Springs	LL4	0.23	0.21	0.25
Hamlet	LL4	0.24	–	0.26
Witsand Farm	LL4	0.25	–	0.27
Aldsworth	LL5	0.24	–	0.25
Alat'ameen	LL5	0.25	–	0.25
Olivenza	LL5	0.24	0.18	0.25
Paragould	LL5	0.25	–	0.25
Tuxtuac	LL5	0.26	–	0.24
Bandong	LL6	0.29	0.23	0.26
Cherokee Springs	LL6	0.26	0.22	0.24
Karatu	LL6	0.32	0.24	0.27
Saint-Séverin	LL6	0.27	0.22	0.21
Attarra	L4	0.34	0.25	0.23
Bald Mountain	L4	0.25	0.15	0.27
Rio Negro	L4	0.25	0.15	0.23
Rupota	L4	0.25	0.16	0.24
Ausson	L5	0.22	0.17	0.23
Blackwell	L5	0.27	–	0.25
Cilimus	L5	0.21	–	0.23
Guibga	L5	0.27	0.16	0.24
Mabwe-Khoywa	L5	0.20	0.16	0.24
Malakal	L5	0.26	0.18	0.26
Messina	L5	0.26	0.15	0.25
Apt	L6	0.27	0.20	0.24
Aumale	L6	0.27	0.17	0.24
Karkh	L6	0.26	0.15	0.23
Kunashak	L6	0.26	0.16	0.24
Kyushu	L6	0.29	0.17	0.24
New Concord	L6	0.29	0.19	0.23
Farmville	H4	0.21	0.12	0.23
Forest Vale	H4	0.22	0.15	0.24
Kabo	H4	0.20	0.12	0.24
Marilia	H4	0.19	0.11	0.24
São Jose do Rio Preto	H4	0.24	0.13	0.22
Allegan	H5	0.21	0.13	0.22
Ehole	H5	0.21	0.15	0.24
Itapicuru-Mirim	H5	0.21	0.12	0.23
Lost City	H5	0.23	0.14	0.24
Primbram	H5	0.23	0.14	0.22
Schenectady	H4	0.20	0.14	0.22
Uberaba	H5	0.25	0.14	0.24
Andura	H6	0.16	0.22	0.23
Bustura	H6	0.18	0.17	0.23
Canon City	H6	0.20	0.15	0.23
Chiang Khan	H6	0.20	0.13	0.23
Guarena	H6	0.18	0.13	0.23
Ipiranga	H6	0.20	0.15	0.23

Errors are the same as those in Table 2.
[a] Normative cpx/(opx + cpx) ratios are from abundances in McSween et al. (1991); – indicates a sample for which norms have not been calculated.

relative abundances of high-calcium pyroxene to total pyroxene from reflectance spectra.

5. Discussion

Since the first comprehensive study of ordinary chondrite spectra was completed (Gaffey, 1976), the ongoing search for the parental asteroids of the ordinary chondrite has centered on the S(IV) subgroup, one of seven subgroups of the S-type asteroids (Gaffey et al., 1993). The S-type asteroids represent a suite of mixtures ranging in composition from pure olivine to pure pyroxene (with potential meteorite analogues including ureilites [S(II)], lodranites [S(III) and S(V)], and mesosiderites [S(VII)] (Gaffey et al., 1993). The S(IV) subgroup is thought to contain objects with mineralogies similar to the ordinary chondrites (Gaffey et al., 1993). The S(IV) Asteroid 6 Hebe has been hypothesized to be the parent body of the H chondrites (Gaffey and Gilbert, 1998),

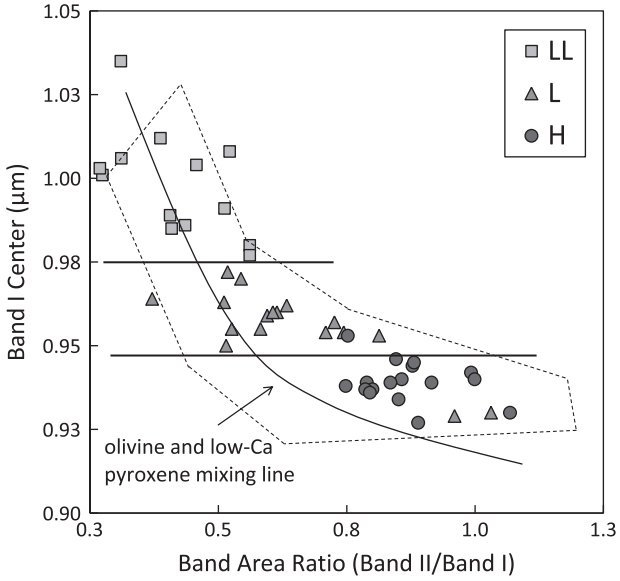

Fig. 2. Current classification for S(IV)-type asteroids modified from Gaffey et al. (1993) and Gaffey and Gilbert (1998). The curve represents a simple mixing line between olivine and low-Ca pyroxene (Gaffey et al., 1993). Spectral characteristics of 48 ordinary chondrites measured in this study are plotted on the diagram. The H, L, and LL chondrites appear to form linear trends, shown as bolded horizontal lines, in which each group defines a relatively restricted range of Band I center and a wider range of band area ratio that appears to mirror the criterion (e.g., FeO in mafic silicates) originally used to distinguish the chemical groups of ordinary chondrites.

and the Flora Family has been suggested as possible source of the L chondrites (Nesvorný et al., 2002). In addition, a large portion of studied Near Earth Asteroids (NEAs) have reflectance spectra similar to ordinary chondrites (Thomas and Binzel, 2009). Like the S(IV) asteroids, ordinary chondrites scatter along a mixing line between olivine and low-Ca pyroxene when plotted in band area ratio vs. Band I center space (Fig. 2). This representation suggests that ordinary chondrites form a nearly continuous sequence between olivine-rich LL chondrites and relatively pyroxene-rich H chondrites (Gaffey et al., 1993).

Examination of the ordinary chondrite spectral data from this study (Fig. 2) suggests that there is an alternative interpretation; the H, L, and LL chondrites appear to form linear trends, in which each group defines a relatively restricted range of Band I center and a wider range of band area ratio. We suggest that this distinction mirrors the criterion (e.g., FeO in mafic silicates) originally used to distinguish the chemical groups of ordinary chondrites. Because BAR is a measure of olivine and pyroxene abundances, it should be proportional to ol/(ol + px) ratios, a relationship which was confirmed earlier in the paper. Given this proportionality, two meteorites with identical BARs should have, within error, identical ol/(ol + px) ratios. If they have identical ol/(ol + px) ratios, Band I center should be controlled almost entirely by the abundance of FeO in olivine and pyroxene. We can test this hypothesis using the 38 chondrite samples for which both modal abundances and silicate mineral compositions were analyzed.

The relationship between measured FeO in mafic minerals and Band I center is shown in Figs. 3a and 4a. Fig. 3a demonstrates that a correlation exists between fayalite (Fa) in olivine and Band I center, which is best described by a second order polynomial fit:

$$\mathrm{Fa} = -1284.9 \times (\mathrm{BIC})^2 + 2656.5 \times (\mathrm{BIC}) - 1342.3, \quad (6)$$

with a R^2 of 0.92. Two L chondrites (Ausson and Bald Mountain) were not included in this correlation due to their anomalous Band I centers. As shown in Fig. 3b, Fa values derived from this equation correlate well with measured Fa, with slight positive offsets for

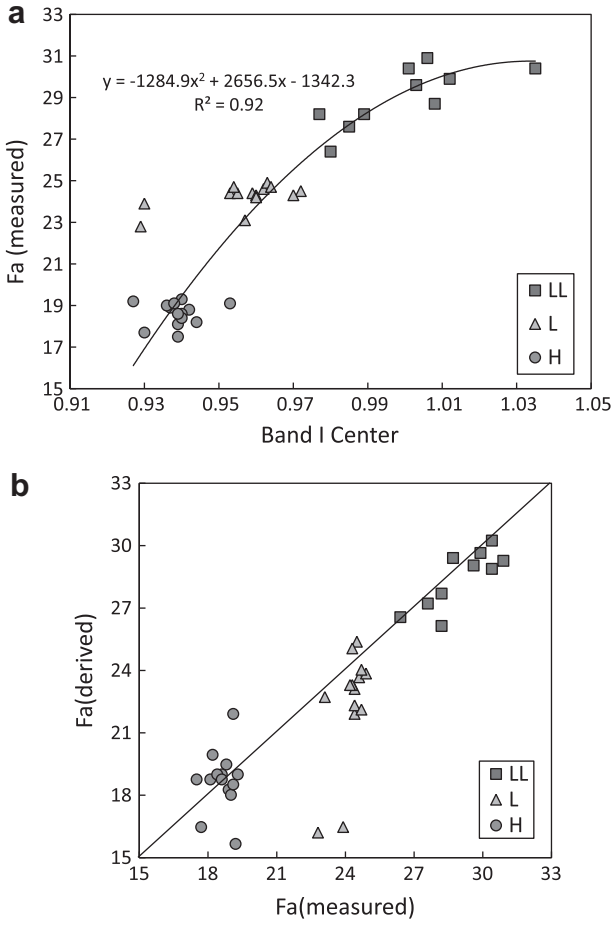

Fig. 3. For the 38 chondrite samples for which both modal abundances and mineral compositions were analyzed, (a) mol% Fa in olivine plotted as a function of Band I center demonstrates that a correlation exists between fayalite (Fa) in olivine and Band I center, and (b) measured vs. derived Fa values correlate reasonably well with measured Fa, with slight positive offsets for derived H chondrite compositions and very slight negative offsets for L and LL chondrites. The correlation between Fa and Band I center allows us to interpret asteroid spectra not simply in the context of BAR vs. Band I center, but in the context of FeO vs. ol/(ol + px) ratios.

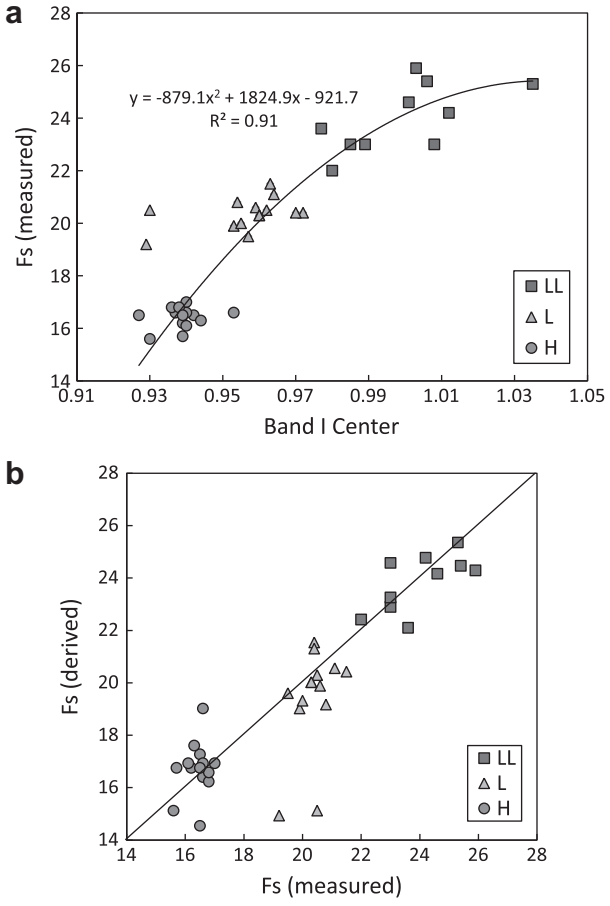

Fig. 4. As with Fa in olivine, (a) mol% Fs in orthopyroxene plotted as a function of Band I center demonstrates that a correlation exist between Fs in pyroxene and Band I center, and (b) derived Fs values correlate well with measured values, with slight offsets in the Hs and LLs. Because of the correlations between Fa and Band I and Fs and Band I, there also appears to be a good correlation between Fa and Fs.

most derived H chondrite compositions and very slight negative offsets for L and LL chondrites. A similar conclusion is reached for ferrosilite (Fs) in pyroxene (Fig. 4a), which correlates with Band I center by a second order polynomial fit:

$$\mathrm{Fs} = -879.1 \times (\mathrm{BIC})^2 + 1824.9 \times (\mathrm{BIC}) - 921.7, \quad (7)$$

with a slightly lower R^2 of 0.91. Again, L chondrites Ausson and Bald Mountain were not included in this correlation. Like derived Fa values, derived Fs values (Fig. 4b) show slight positive offsets for H chondrites and slight negative offsets for L and LL chondrites. However, because both Fa and Fs in mafic silicates correlate well with Band I center, there also appears to be a well-established correlation between Fa and Fs.

Along with the previously established linear relationship between BAR and ol/(ol + px), the correlation between mafic silicate compositions (Fa, Fs) and Band I center allows us to interpret S(IV) asteroid spectra not simply in the context of BAR vs. Band I center, but in the context of FeO vs. ol/(ol + px) ratios – the same criteria used to classify ordinary chondrites. Figs. 5a and 6a show mol% Fa and mol% Fs, respectively, plotted as a function of ol/(ol + px). Dashed boxes represent the range of XRD-measured ol/(ol + px) (from this study) and the range of measured Fa and Fs contents in ordinary chondrites (Brearley and Jones (1998) and references therein). In each plot, the H, L, and LL chondrites are clearly separated in mafic silicate composition and exhibit only minimal overlap in ol/(ol + px). In Figs. 5b and 6b, we plot the spectrally-derived ol/(ol + px) vs. derived Fa or Fs compositions (calculated using Eqs. (6) and (7), respectively). Dashed boxes are the same as those in Figs. 5a and 6a. The solid grey boxes represent the least root mean square of the errors on these spectrally-derived values (0.03 for ol/(ol + px), 1.3 mol% for Fa, and 1.4 mol% for Fs). Our calibrations and their associated errors are presented in Table 4.

If we classified the meteorites in this study using only spectrally-derived mineral abundances and silicate compositions, we would correctly classify 86% of H chondrites (12/14), 77% of L chondrites (10/14) and 100% of LL chondrites (10/10). If the solid boxes, which account for the RMS error, are used as parameters for classification instead, all but two the L chondrites outliers could be correctly classified. However, if these calibrations were applied to additional samples, the overlap between L and LL chondrites implied by our derived data, and suggested by previous authors based on mineral chemistries (e.g., Rubin, 1990), may make some L and LL chondrites difficult to classify.

The correct classification of 83% of the ordinary chondrites in this study indicates that similar success would be expected when attempting to determine the mineralogies of S(IV) asteroids. This statement is true, but it is not without caveats. First, these calibrations are only useful for samples with chondrite-like mineralogies and chemistries. When applying these calibrations to asteroid

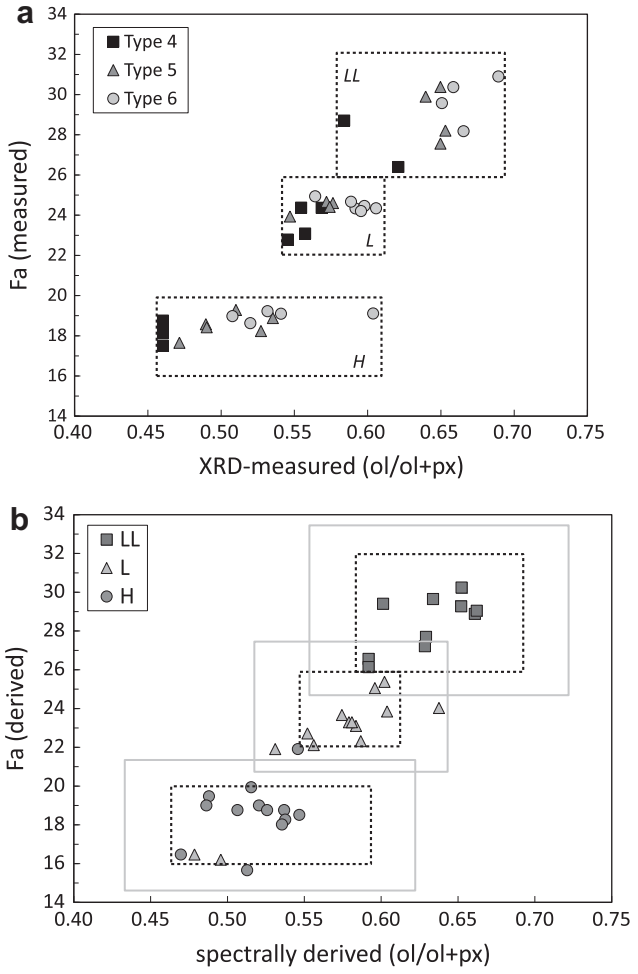

Fig. 5. (a) Mol% Fa plotted as a function of ol/(ol + px) in the 38 chondrite samples for which both modal abundances and mineral compositions were analyzed, and (b) spectrally-derived Fa compositions vs. derived ol/(ol + px). Dashed boxes represent the range of XRD-measured ol/(ol + px) (from this study) and the range of measured Fa contents in ordinary chondrites (Brearley and Jones (1998) and references therein). The solid boxes include the least square root mean of the errors on these spectrally-derived values (0.03 for ol/(ol + px) and 1.3 mol% for Fa). Based on derived Fa content and ol/(ol + px), we can correctly classify 86% of H chondrites, 71% of L chondrites, and 100% of LL chondrites.

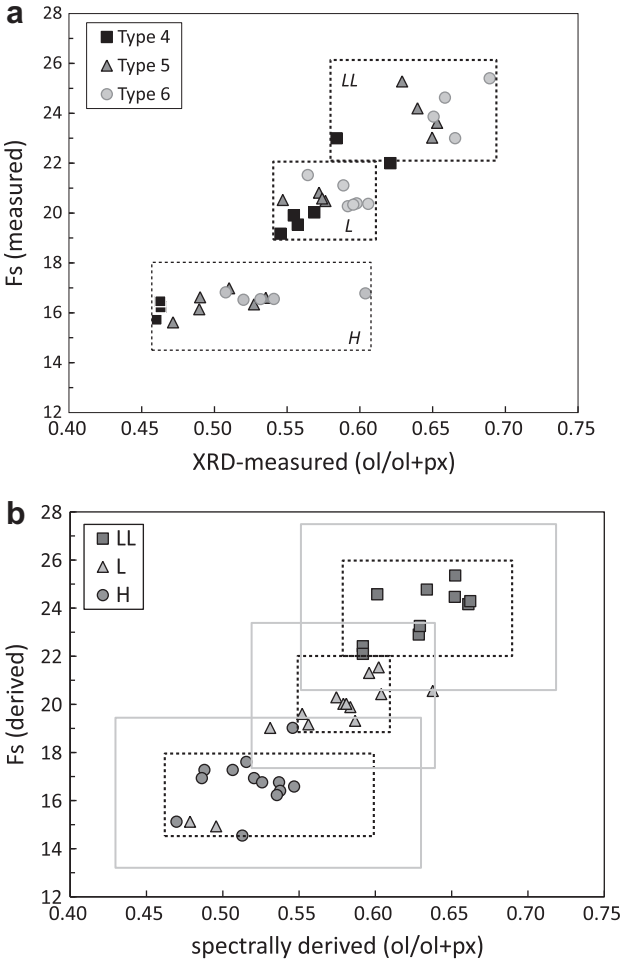

Fig. 6. (a) Mol% Fs plotted as a function of ol/(ol + px) in the 38 chondrite samples for which both modal abundances and mineral compositions were analyzed, and (b) spectrally-derived Fs compositions vs. derived ol/(ol + px). Dashed boxes represent the range of XRD-measured ol/(ol + px) (from this study) and the range of measured Fs contents in ordinary chondrites (Brearley and Jones (1998) and references therein). The solid boxes include the least square root mean of the errors on these spectrally-derived values (0.03 for ol/(ol + px) and 1.4 mol% for Fs.) Based on derived Fs content and ol/(ol + px), we can correctly classify 86% of H chondrites, 71% of L chondrites, and 100% of LL chondrites.

spectra, one must first be confident that the asteroid in question is an S(IV) type (and a likely chondrite parent body). The S(IV) types can be distinguished from other S-type asteroids on the correlations between spectra slope, band depth, and albedo (Gaffey et al., 1993). In addition, probability models for determining asteroid class and source region (Thomas and Binzel, 2009) have recently been developed that may improve the classification of asteroids, particularly in a large sample group. Secondly, it is also important to consider the possible effects of space weathering processes (Clark et al., 2003). Though asteroid spectra become redder as a result of space weathering, laboratory studies have shown that spectral parameters (i.e. band depth) remain unchanged (Marchie et al., 2005; Sasaki et al., 2001); therefore, interpreted mineralogies and compositions should not be influenced by space weathering (Vernazza et al., 2008).

Moving beyond simple classification, our calibrations may also allow us to determine the geologic histories of some S-type asteroids, specifically whether they are unaltered (ordinary chondrite) or have experienced partial melting (primitive achondrite). One parameter used to decipher this history is spectrally-derived FeO content, where FeO-rich pyroxene is interpreted as an indicator of partial melting and chondrite-like FeO compositions are suggestive of a primitive asteroid. For this parameter to be useful, derived Fs compositions must be accurate. However, calibrations used to determine Fs values in asteroids (Gaffey et al., 2002; Gaffey, 2007) have been shown to yield higher than measured Fs compositions when applied to mixtures of ordinary chondrite-like compositions (McCoy et al., 2007), and their limitations when applied to spectra of ordinary chondrite-like compositions has been acknowledged (Gaffey, 2009). Because our calibrations were derived entirely from ordinary chondrites, they should provide more accurate Fs compositions and may provide some insight into the partial melting debate. One example is the S-type asteroid Itokawa, which has identified as a possible partial melt based on FeO content ($Fs_{43\pm5}$) (Abell et al., 2007) and as an LL-chondrite parent body based on spectral parameters (Abe et al., 2006). Using spectral parameters measured by Thomas and Binzel (2009), we derived an Fs composition of Fs_{25}, which falls into the range of ordinary chondrite FeO values and suggests that partial melting did not occur. When derived ol/ol + px ratios are plotted along with Fs compositions, Itokawa plots in the range defined by the LL chondrites.

Table 4
Summary of calibrations and associated error.

	R^2	RMS		
		ol/(ol + px)	Fa (mol%)	Fs (mol%)
ol/(ol + px) = $-0.424 \times$ BAR + 0.728	0.73	0.03		
Fa = $-1284.9 \times (\text{BIC})^2 + 2656.5 \times (\text{BIC}) - 1342.3$	0.92		1.3	
Fs = $-879.1 \times (\text{BIC})^2 + 1824.9 \times (\text{BIC}) - 921.7$	0.91			1.4

6. Summary

Using visible/near-infrared spectra to establish meteorite–asteroid connections requires a direct comparison between spectral features (e.g., Band I and II centers, band area ratios) in both objects. These comparisons could be made on the basis of criteria primarily used in meteoritics (i.e. silicate mineral compositions and abundances) if relationships were established between spectral parameters and mineralogical parameters. Here we have used a suite of ordinary chondrites, in which spectral and mineralogical data have been measured, to establish such relationships between chondrites and their parent asteroids.

Correlation of mineralogical and spectral parameters in our suite of 38 ordinary chondrites indicates that well-defined relationships exist between Band I center and FeO (as Fa or Fs) and between BAR and ol/(ol + px). Using these parameters, we can correctly classify 32 of 38 ordinary chondrites from VIS/NIR spectra. This suggests that ~80% of known S(IV) asteroids should be correctly classified as potential H, L, or LL parent bodies using spectrally-derived silicate mineral compositions and abundances. With these tools, we can move beyond band parameters to directly discussing asteroid and meteorite properties using a common language of mineral abundance and composition.

Acknowledgments

We would like to thank Gordon Cressey, at the Natural History Museum in London, for his assistance in the collection and interpretation of XRD modal data, and Takahiro Hiroi, at Brown University's Keck/NASA Reflectance Experiment Laboratory (RELAB), for collecting VNIR spectra of several samples examined in this study. Thanks also to the Smithsonian Institution and the Natural History Museum for providing powder samples for modal and spectral analysis. We would also like to thank Tom Burbine and Vishnu Reddy for their helpful reviews, which greatly improved this manuscript. This work was supported by NASA through cosmochemistry Grant NNG06GG36G to H.Y.M. and planetary geology and geophysics Grant NNX06AH69G to J.M.S.

References

Abe, M., and 12 colleagues, 2006. Near-infrared spectral results of Asteroid Itokawa from the Hayabusa spacecraft. Science 312, 1334–1338.

Abell, P.A., Vilas, F., Jarvis, K.S., Gaffey, M.J., Kelley, M.S., 2007. Mineralogical composition of (25143) Itokawa 1998 SF36 from visible and near-infrared reflectance spectroscopy: Evidence for partial melting. Meteorit. Planet. Sci. 42, 2165–2177.

Adams, J.B., 1974. Visible and near-infrared diffuse reflectance spectra of pyroxenes as applied to remote sensing of solid objects in the Solar System. J. Geophys. Res. 79, 4829–4836.

Adams, J.B., 1975. Interpretation of visible and near-infrared diffuse reflectance spectra of pyroxene and other rock-forming minerals. In: Karr, C., III (Ed.), Infrared and Raman Spectroscopy of Lunar and Terrestrial Minerals. Academic Press, New York, pp. 91–116.

Batchelder, M., Cressey, G., 1998. Rapid, accurate phase quantification of clay-bearing samples using a position sensitive X-ray detector. Clays Clay Mineral. 46, 183–194.

Burbine, T.H., McCoy, T.J., Jarosewich, E., Sunshine, J.M., 2003. Deriving asteroid mineralogies from reflectance spectra: Implications for the MUSES-C target asteroid. Antarct. Meteor. Res. 16, 185–195.

Burns, R.G., 1970. Crystal field spectra and evidence of cation ordering in olivine minerals. Am. Mineral. 55, 1608–1632.

Burns, R.G., Huggins, F.E., Abu-Eid, R.M., 1972. Polarized absorption spectra of single crystals of lunar pyroxenes and olivine. Moon 4, 93–102.

Clark Jr., S.P., 1957. Absorption spectra of some silicates in the visible and near-infrared. Am. Mineral. 42, 732–742.

Clark, B.E., Hapke, B., Pieters, C., Britt, D., 2003. Asteroid space weathering and regolith evolution. In: Botke, W.F., Jr., Cellino, A., Paolicchi, P., Binzel, R.P. (Eds.), Asteroids III. The University of Arizona Press, Tucson, pp. 585–599.

Clayton, R.N., Mayeda, T.K., Goswami, J.N., Olsen, E.J., 1991. Oxygen isotope studies of ordinary chondrites. Geochim. Cosmochim. Acta 55, 2317–2337.

Cloutis, E.A., 1985. Interpretive Techniques for Reflectance Spectra of Mafic Silicates. M.S. Thesis, University of Hawaii, Honolulu, Hawaii, USA.

Cloutis, E.A., Gaffey, M.J., 1991. Pyroxene spectroscopy revisited: Spectral–compositional correlations and relationships to geothermometry. J. Geophys. Res. 91, 11641–11653.

Cloutis, E.A., Gaffey, M.J., Jackowski, T.L., Reed, K.L., 1986. Calibration of phase abundance, composition, and particle size distribution for olivine–orthopyroxene mixtures from reflectance spectra. J. Geophys. Res. 91, 11641–11653.

Cressey, G., Schofield, P.F., 1996. Rapid whole-pattern profile stripping methods for the quantification of multiphase samples. Powder Diffract. 11, 35–39.

Cross, W., Cross, J.P., Pirsson, L.V., Washington, H.S., 1902. A quantitative chemico-mineralogical classification and nomenclature of igneous rocks. J. Geol. 10, 555–690.

Dodd, R.T., 1981. Meteorites: A Petrologic–Chemical Synthesis. Cambridge Univ. Press, Cambridge, UK. 377pp.

Dunn, T.L., Cressey, G., McSween Jr., H.Y., McCoy, T.J., 2010. Analysis of ordinary chondrites using powder X-ray diffraction: 1. Modal mineral abundances. Meteorit. Planet. Sci. doi:10.1111/j.1945-5100.2009.01011.x.

Dunn, T.L., McSween Jr., H.Y., McCoy, T.J., Cressey, G., 2010. Analysis of ordinary chondrites using powder X-ray diffraction: 2. Applications to ordinary chondrite parent body processes. Meteorit. Planet. Sci. doi:10.1111/j.1945-5100.2009.01012.x.

Gaffey, M.J., 1976. Spectral reflectance characteristics of the meteorite classes. J. Geophys. Res. 81, 905–920.

Gaffey, M.J., 2007. One pyroxene? Two pyroxenes? Three pyroxenes? Pyroxene composition from asteroid spectra. Lunar Planet. Sci. 38. Abstract #1338 (CD-ROM).

Gaffey, M.J., 2009. Identifying asteroidal ordinary chondrite assemblages and petrographic types form VNIR spectra. Lunar Planet. Sci. 48. Abstract #1412 (CD-ROM).

Gaffey, M.J., Gilbert, S.L., 1998. Asteroid 6 Hebe: The probable parent body of the H-type ordinary chondrites and the IIE iron meteorites. Meteorit. Planet. Sci. 33, 1281–1295.

Gaffey, M.J., Bell, J.F., Brown, R.H., Burbine, T.H., Piateck, J.L., Reed, K.L., Chaky, D.A., 1993. Mineralogical variations within the S-type asteroid class. Icarus 10, 573–602.

Gaffey, M.J., Cloutis, E.A., Kelley, M.S., Reed, K.L., 2002. Mineralogy of asteroids. In: Bottke, W.F., Jr., Cellino, A., Paolicchi, P., Binzel, R.P. (Eds.), Asteroids III. The University of Arizona Press, Tucson, pp. 83–204.

Gastineau-Lyons, H.K., McSween Jr., H.Y., Gaffey, M.J., 2002. A critical evaluation of oxidation versus reduction during metamorphism of L and LL group chondrites, and implications for asteroid spectroscopy. Meteorit. Planet. Sci. 37, 75–89.

Jarosewich, E., 1990. Chemical analyses of meteorites: A compilation of stony and iron meteorite analyses. Meteoritics 25, 323–337.

Jarosewich, E., 2006. Chemical analyses of meteorites at the Smithsonian Institution: An update. Meteorit. Planet. Sci. 41, 1381–1382.

Keil, K., Haack, H., Scott, E.D., 1994. Catastrophic fragmentation of asteroids: Evidence from meteorites. Planet. Space Sci. 42, 1109–1122.

King, T.V., Ridle, W.I., 1987. Relation of the spectroscopic reflectance of olivine to mineral chemistry and some remote sensing applications. J. Geophys. Res. 92, 11457–11469.

Marchie, S., Brunetto, R., Magrin, S., Lazzarin, M., Gandolfi, D., 2005. Space weathering of near-Earth ad main belt silicate-rich asteroids: Observations and ion irradiation experiments. Astron. Astrophys. 443, 769–775.

McCoy, T.J., Corrigan, C.M., Sunshine, J.M., Bus, S.J., Gale, A., 2007. Does asteroid spectroscopy provide evidence for widespread partial melting of asteroids? II. Pyroxene compositions. Lunar Planet. Sci. 38. Abstract #1631 (CD-ROM).

McSween Jr., H.Y., Bennett, M.E., Jarosewich, E., 1991. The mineralogy of ordinary chondrites and implications for asteroid spectrophotometry. Icarus 90, 107–116.

Nesvorný, D., Morbidelli, A., Vokrouhlicky, D., Bottke, W.F., Broz, M., 2002. The flora family: A case of the dynamically dispersed collisional swarm? Icarus 157, 155–172.

Pieters, C.M., Hirio, T., 2004. RELAB (Reflectance Experiment Laboratory): A NASA multiuser spectroscopy facility. Lunar Planet. Sci. 35. Abstract #1720 (CD-ROM).

Rubin, A.E., 1990. Kamacite and olivine in ordinary chondrites: Intergroup and intragroup variations. Geochim. Cosmochim. Acta 54, 1217–1232.

Sasaki, S., Nakamura, K., Hamabe, Y., Kurahashi, E., Hirio, T., 2001. Production of iron nanoparticles by laser irradiation in a simulation of lunar-like space weathering. Nature 410, 555–557.

Sunshine, J.M., Pieters, C.M., 1998. Determining the composition of olivine from reflectance spectroscopy. J. Geophys. Res. 103, 13675–13688.

Sunshine, J.M., Bus, S.J., McCoy, T.J., Burbine, T.H., Corrigan, C.M., Binzel, R.P., 2004. High-calcium pyroxene as an indicator of igneous differentiation in asteroids and meteorites. Meteorit. Planet. Sci. 39, 1343–1357.

Thomas, C.A., Binzel, R.P., 2009. Identifying meteorite source regions through near-Earth object spectroscopy. Icarus. doi:10.1016/j.icarus.2009.08.008.

Van Schmus, W.R., Wood, J.A., 1967. A chemical–petrologic classification for the chondrite meteorites. Geochim. Cosmochim. Acta 31, 747–765.

Vernazza, P., Binzel, R.P., Thomas, C.A., DeMeo, F.E., Bus, S.J., Rivikin, A.S., Tokunaga, A.T., 2008. Compositional difference between meteorites and Near-Earth Asteroids. Science 454, 858–860.